Carbohydrate Polymers 86 (2011) 732–741

Contents lists available at ScienceDirect

Carbohydrate Polymers

journal homepage: www.elsevier.com/locate/carbpol

Biopolymers-based nanocomposites: Membranes from propionated lignin and cellulose for water purification

Laura Manjarrez Nevárez [a], Lourdes Ballinas Casarrubias [b,*], Oscar Solís Canto [a], Alain Celzard [c], Vanessa Fierro [c], Rigoberto Ibarra Gómez [a], Guillermo González Sánchez [a]

[a] Centro de Investigación en Materiales Avanzados, S.C., Laboratorio Nacional de Nanotecnología, Miguel de Cervantes No. 120, Chihuahua, Chih. 31109, Mexico
[b] Facultad de Ciencias Químicas, Universidad Autónoma de Chihuahua, Circuito Universitario s/n, Campus Universitario No. 2, C.P. 31125, Chihuahua, Chih., Mexico
[c] Institut Jean Lamour - UMR CNRS 7198, CNRS - Nancy-Université - UPVM, ENSTIB, 27 rue du Merle Blanc, BP 1041, 88051 Epinal Cedex 9, France

ARTICLE INFO

Article history:
Received 8 March 2011
Received in revised form 27 April 2011
Accepted 12 May 2011
Available online 27 May 2011

Keywords:
Membranes
SKPM
Nanocomposites
Lignin
Biopolymers

ABSTRACT

Nanocomposite membranes for water treatment were prepared by vapor-induced phase separation method from propionated lignin and cellulose triacetate (CTA). Three kinds of lignin were used: Kraft, Organosolv and Hydrolytic, which were propionated for improving their compatibility with CTA. Such chemical lignin modification was analyzed by FTIR, UV spectrophotometry and GPC. Morphology (through FE-SEM and AFM), mechanical properties (DMA), and surface potential (SPKM) were investigated for all membranes obtained. For determining membrane performance, groundwater from Chihuahua (Mexico) containing high concentrations of fluoride, arsenic, calcium, sodium and magnesium, was filtrated. Membrane rejection was 15–35% for anions present, and 12–42% and 27–54% for monovalent and divalent cations, respectively. Arsenic and fluoride removal by membranes was found to be affected by ionic and organic matter present in groundwater.

1. Introduction

Agro-industrial waste is the most abundant renewable resource residue on Earth. Accumulation of this biomass in large quantities every year results not only in environmental deterioration, but also represents an economic problem for companies. Every year, approximately 10–50 billion dry tons per year of lignocellulosic wastes are produced worldwide (Sims, Michael, Jack, & Warren, 2008). Nevertheless, a number of valuable commercial products, such as activated carbons (Fierro, Torné Fernández, & Celzard, 2006; Pandey, Soccol, Nigam, & Soccol, 2000), biosurfactants (Mercade & Manresa, 1994), and phenolic resins (Stewart, 2008), may be prepared from these materials.

Additionally, composites derived from natural organic materials have received considerable attention because of their properties: high specific strength and modulus, low cost/high-volume applications, low density compared to composites reinforced by inorganic materials, low energy consumption, easy processability, renewable origin and possibility of recycling (Kiziltas, Gardner, Han, & Yang, 2010; Oksman, Mathew, Bondeson, & Kvien, 2006). Biocomposites have gained important consideration in this field (Alexy, Kosikova, & Podstranska, 2000; Kamel, 2007; Le Digabel & Avéous, 2006), due to their oxidation resistance, thermal behavior, and good mechanical resistance (Alemdar & Sain, 2008; Chen, Liu, Chang, Cao, & Anderson, 2009).

Recently, all-biopolymer based films have been reported for membrane applications (Manjarrez Nevárez et al., this issue). Heavy metals in groundwater used for human intake are of international concern due to their well known toxicity (Faust & Aly, 1998). Therefore, there is a high demand for applying efficient methods and materials for metal removal from drinking water. Due to their efficiency, low operating cost and high selectivity, membrane processes are at the forefront of technology separation (Drioli & Romano, 2001).

Mechanical and hydraulic properties are the most important parameters that should be considered in membrane manufacturing. Cellulosic ester materials are among the best polymers for preparing organic membranes (El-Saied, Basta, Barsoulm, & Elberry, 2003), and are indeed used in reverse osmosis (Edgar et al., 2001; Haddad, Ferjani, Roudesli, & Deratani, 2004), ultrafiltration (Ballinas Casarrubias et al., 2006) and pervaporation (Wang, Li, Li, & Chen, 2007) processes. These materials are obtained from different raw materials such as cotton, recycled paper and sugar cane bagasse

* Corresponding author. Tel.: +52 6142366000; fax: +52 6142366000.
E-mail addresses: laura.manjarrez@cimav.edu.mx (L. Manjarrez Nevárez), mballinas@uach.mx, lourdes.ballinas@gmail.com (L. Ballinas Casarrubias), oscar.solis@cimav.edu.mx (O.S. Canto), alain.celzard@lcsm.uhp-nancy.fr (A. Celzard), vanessa.fierro@lcsm.uhp-nancy.f (V. Fierro), rigoberto.ibarra@cimav.edu.mx (R. Ibarra Gómez), guillermo.gonzalez@cimav.edu.mx (G. González Sánchez).

0144-8617/$ – see front matter © 2011 Elsevier Ltd. All rights reserved.
doi:10.1016/j.carbpol.2011.05.014

(Park, Misra, Drzal, & Mohanty, 2004). Due to their origin, cheap acetylated polymers to be marketed for membrane production could be produced with different degrees of acetylation (DS). Nevertheless, these materials present some operational disadvantages, such as narrow pH and temperature operating ranges that are not suitable for more aggressive cleaning, low mechanical strength and poor resistance to oxidation and to fouling (Andrade Molinar, 2007; Arthanareeswaran, Thanikaivelan, Srinivasn, Mohan, & Rajendran, 2004; Kosutic, Kstelan Kunst, & Kunst, 2000). For these reasons, modification of the cellulose acetate is required for improving membrane properties. In the present work, cellulose triacetate is employed because its mechanical behavior and biofouling resistance are higher than those of cellulose diacetate (Ruehr et al., 2010). Lower fluxes are attained with CTA than with lower DS acetylated materials (El-Saied et al., 2003), but higher salt rejection is observed (Baker, 2004).

Lignin is a biopolymer which has a complex chemical structure that depends on a number of factors, including botanical origin, environmental growth conditions and extraction conditions. However, lignins are polar polymers and thus exhibit a very poor solubility in apolar media and processability of these have limited their applications (Pouteau, Dole, Cathala, Averous, & Boquillon, 2003; Wu, Wang, Li, Li, & Wang, 2009). Chemical modification is an alternative for changing solubility behavior and getting higher polymer-lignin compatibility (Thielemans & Wool, 2005). Lignin incorporation into polypropylene and polystyrene (Pucciariello, Villani, Bonini, D'Auria, & Vetere, 2004), and in polyethylene terephthalate (Canetti & Bertini, 2007) was reported. In such composites, a reinforcement effect was always observed (Baumberger, Lapierre, Monties, & Della Valle, 1998; Gregorová, Cibulková, Kosiková, & Símon, 2005). For instance, modified lignin compatibility will be superior with cellulose acetate having the highest DS.

The objective of the present work is pursuing the investigation of all-biopolymer nanocomposite synthesis using cellulose-lignin matrices for membrane applications. Propionated material using three kinds of lignins: Kraft, Organosolv and Hydrolytic, was added to cellulose triacetate polymers by the evaporation-precipitation method. These materials were tested in a continuous flow cell for drinking water treatment.

2. Methodology

2.1. Lignin esterification

Lignin used in this work was provided by Sigma–Aldrich as Kraft (KL), Organosolv (OL) and hydrolytic (HL) lignin. All of them were propionated according to the procedure described elsewhere (Thielemans & Wool, 2005), leading to PKL, POL and PHL materials, respectively. Briefly, esterification reactions were carried out at 50 °C with propionic anhydride (Sigma–Aldrich) under nitrogen atmosphere, using 4-dimethyl amino pyridine (4-DMAP) as catalyst. The mixtures, based on a 2:1 weight ratio of anhydride to lignin and 0.05 g of 4-DMAP per gram of lignin, were stirred vigorously for 2 h, and left to react for 8 h. Addition of diethyl ether (10 mL) quenched the reaction by precipitating KL once esterified. OL and HL were precipitated after cooling with ice. The three kinds of lignins were washed with methanol and deionized water. The aqueous phase was drained in order to remove all the remaining catalyst.

2.2. Characterization of esterified lignin

2.2.1. Determination of phenolic hydroxyl content by UV spectrophotometry

Lignin absorbs in the UV region between 200 and 380 nm because of its aromatic nature. The method consisted in ionizing phenolic groups with alkali solution and observing a bathochromic and hyperchromic effects in the absorption spectrum. Differential absorption spectra, expressing the difference between the spectra of ionized and non ionized samples, were obtained, from which the OH content of each kind of lignin could be measured before and after esterification (Goldschmid, 1954).

A Lambda 900 Perkin Elmer UV/Vis spectrometer was used in the following conditions: wavelength range 200–400 nm, slit 1 nm, scan speed 250 nm min^{-1}. Spectra were acquired for all lignins in alkaline solution. For that purpose, 0.015 g of lignin sample was dissolved in 30 mL of a water:dioxane mixture (weight ratio of 1:2) which was next diluted with water. pH adjustment was made with sodium hydroxide aqueous solution.

2.2.2. Fourier Transformed Infrarred spectrometry (FTIR)

FTIR spectroscopy was performed using a Perkin Elmer FTIR spectrometer, with a deuterated triglycine sulfate (DTGS) detector and a potassium bromide (KBr) beam splitter. A total of 25 cumulative scans were taken with a resolution of 2 cm^{-1} in transmission mode. A small amount of lignin dispersed or dissolved in acetone was deposited on the ATR (attenuated total reflectance) instrument of the spectrometer.

2.2.3. Gel permeation–high performance liquid chromatography (GPC–HPLC) analysis

All lignin samples, raw and acetylated, were analyzed by an Alliance 2695 GPC–HPLC system using an ultraviolet detector and a PL gel 5 MIXED-C 300 mm × 7.5 mm (Polymer Laboratories) column. The column (pore sizes 10^4 and 10^5 Å) allowed determining molecular weights ranging from 0.2 to 2000 kDa. The column was operated at a flow rate of 1 mL min^{-1} and was calibrated with polystyrene standards over the range of molecular weights of studied lignin.

Lignin samples were dissolved in THF with 0.1 M LiCl for GPC (100 mg of lignin per 3 mL of THF/LiCl solution). LiCl was used for avoiding the association of lignin molecules, even modified, that has been found to significantly increase the measured weight average molecular mass and polydispersity, and that might result in solvent-dependent molecular weights (Connors, Sarkanen, & McCarthy, 1980).

2.3. Nanocomposite synthesis

Nanocomposites were prepared by solution casting using CH_2Cl_2 (Sigma–Aldrich) as solvent. For membrane preparation, relative humidity (RH) and temperature (T) were varied at 3 levels: 10, 30, 70% RH and 35, 45, 55 °C, respectively, using a controlled humidity chamber (Shell Lab). Films were prepared either without lignin or with 1 wt.% of propionated lignin. Cellulose triacetate (Sigma–Aldrich) and propionated lignin nanoparticles were separately dissolved into methylene chloride (3.3 and 0–1 wt.%, respectively) and stirred at controlled temperature (25 °C) for 2 h. Solutions were next mixed to obtain the casting one. The casting solutions were uniformly spread over a glass dish of 14 cm × 19 cm. Precipitation by solvent evaporation was performed in controlled RH and T conditions as mentioned above, during 2 h each. Then, samples were immersed in a water bath for being removed from the glass dishes, dried and stored in dry conditions at room temperature.

2.4. Nanocomposite analysis

2.4.1. Field emission scanning electron microscopy (FE-SEM)

Membrane morphology was investigated by FE-SEM, JSM 7401F (JEOL). Samples were first metalized with gold (Denton Desk-II

Gatan), and micrographs were taken at 1 kV acceleration voltage. Top view structures were analyzed at magnification of 25,000×.

2.4.2. Atomic force and scanning Kelvin probe microscopy (AFM and SKPM)

AFM analyses were performed in a Nanoscope IV, Digital Instrument. Samples without any pretreatment were installed onto stainless steel disc with adhesive tape in a sample holder. Images were obtained in tapping mode using a silicum tip doped with antimony (TESP Veeco®). These tips had their optimal frequency range between 272 and 334 kHz. The scan rate was around 1 Hz. A feedback loop maintained a constant oscillation amplitude by moving the scanner vertically at every *x*, *y* data point. Recording this movement formed the topographical image. Resolution was 512 × 512 pixels. Image processing and determination of the root mean square roughness (R_{rms}) were obtained using the WSxM software (Horcas et al., 2007).

The distribution of electrical potential at the membrane surface was measured with SKPM technique, using the same Nanoscope IV instrument. Surface potential detection is a two-pass procedure wherein the surface topography is obtained by standard tapping mode (see above) in the first pass, and the surface potential is measured during the second pass. In the first pass in tapping mode, the cantilever is mechanically vibrated near its resonant frequency by a small piezoelectric element. The latter is switched off in the second pass, and an oscillating voltage of the form $V_{DC} + V_{AC} \cos \omega t$ is, where the DC voltage is adjustable, is applied directly to the probe tip. Any DC voltage difference between the tip and the sample surface produces an oscillatory electric force on the cantilever. This causes the cantilever to vibrate, and the corresponding amplitude is detected. The force vanishes when the DC voltage applied to the tip is changed at a value equal to the surface potential of the sample. The latter can thus be measured, and is plotted versus *x*, *y* coordinates, creating a 3D surface potential image (Serry et al., 2004).

2.4.3. Mechanical properties of nanocomposites

Tensile testing of films was carried out in a Dynamic Mechanical Analyzer (DMA) RSA III from TA Instruments. The tests were performed at constant temperature of 25 °C, using a traction rate of 0.005 mm s^{-1}. Sample had initial dimensions of 8 mm and 0.384 mm^2 in length and cross-sectional area, respectively. The tensile modulus was calculated by the instrument software from the slope of the initial portion of the stress–strain curves. The resultant mechanical properties were averaged over at least three specimens of each kind of film.

2.4.4. Contact angle measurement

Contact angle measurement is widely used to characterize the hydrophilic property of polymer surfaces, including polymeric membranes (Asatekin, Kang, Elimelech, & Mayes, 2007). In the experiment, contact angle between water and membrane surface was measured by the sessile drop method using an FTA-32 goniometer (Firsttenangstroms). A water droplet was placed onto the membrane surface using a syringe, and contact angle of droplet was measured. The values reported here are averages of 3 separate analyses on the same membrane.

2.4.5. Thermogravimetric analysis (TGA)

Thermogravimetric measurements were made on a TA Instrument STD Q500. The microbalance had a precision of ± 0.1 μg and was kept at constant temperature during analyses to avoid the variation of weight measurement with temperature. Samples of about 10 (±3) mg were placed into alumina pans. The samples were heated from 25 °C to 100 °C at 5 °C min^{-1} under angon flowing at 60 mL min^{-1} for 60 min. At least three replicates were done for each sample for determinating their water content.

Table 1
Composition of groundwater form Chihuahua, Mexico well.

Parameter	Units	Values
Turbidity	NTU[a]	1
Conductivity	μS cm^{-1}	723
pH	–	7.17
Temperature	°C	25
Calcium	mg L^{-1}	8.75
Sodium	mg L^{-1}	250
Potassium	mg L^{-1}	0.956
Magnesium	mg L^{-1}	0.440
Fluoride	mg L^{-1}	11.8
Arsenic	mg L^{-1}	0.435
TSD[b]	mg L^{-1}	706

[a] Nephelometric turbidity units.
[b] Total solid dissolved.

2.4.6. Permeability tests

Membrane permeability was measured using an Osmonics SEPA flat-sheet, cross-flow, test cell with an effective area of 0.014 m^2. The cell was operated at room temperature in a recirculating mode, with a feed solution drawn from a 2 L reservoir and returned to the reservoir after passing throughout the test cell. Each membrane was conditioned by passing distilled water through the system until the flow was stabilized. The performance, or efficiency, of the nanocomposite membranes prepared in this work was evaluated from two parameters: selectivity and trans-membrane flow. The latter, often denoted as the flux or permeation rate, was defined as the volume flowing throughout the membrane per unit area, pressure and time (L m^{-2} h^{-1} bar^{-1}). Then, groundwater containing a high arsenic level (0.435 mg L^{-1}) was passed throughout the membrane. Permeated flow was monitored as well as the feed flow pressure. Initial groundwater parameters are shown in Table 1.

The total amount of arsenic in the permeated solution was analyzed by atomic absorption spectroscopy using a hydride generation mode (Perkin Elmer *Analysis 800-FIAS 100)*. Fluoride was analyzed by a potentiometric method based on the Mexican regulation emitted by the Environmental and Natural Resources Secretary: NMX-AA-077-SCFI-2001 (Secretaria del Medio Ambiente y Recursos naturales, 2001a). For calcium and magnesium, flame atomic absorption was used. After the membrane process, calcium, potassium and arsenic were analyzed in the permeate according again to NMX-AA-051-SCFI-2001 (Secretaria del Medio Ambiente y Recursos naturales, 2001b). The amount of salt rejected was calculated using the following equation:

$$\text{Rejection}\,(\%) = \left[1 - \frac{C}{C_0}\right] \times 100 \quad (1)$$

where C is concentration of solute in permeate water (ppm), and C_0 is the concentration of solute in feed water (ppm). Such a calculation was carried out for each membrane put into contact with 1 L of groundwater flowing during 2 h.

3. Results and discussion

3.1. Chemical structure

Chemical modification of lignin with propionic anhydride, replacing hydroxyl groups by propionyl chains, made its surface more hydrophobic, and thus, increased its compatibility with the polymer matrix. Esterification indeed improves the dispersion of lignocellulosic materials into polymeric matrices as well as the dimensional stability at the polymer–filler interface in the final

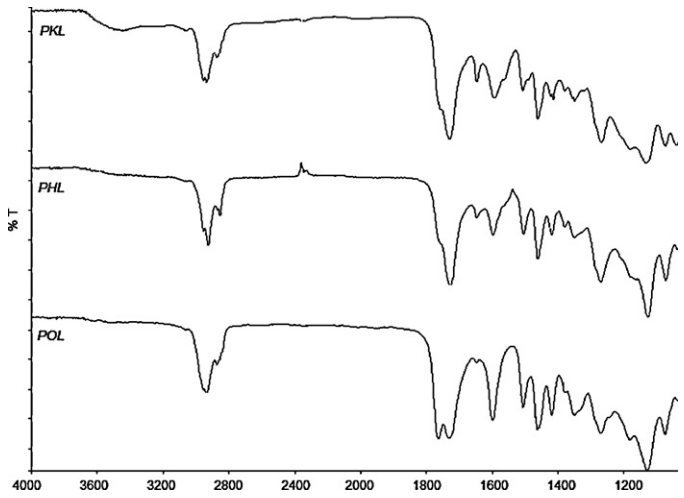

Fig. 1. FTIR spectra of propionated lignin (PKL, POL and PHL).

composite, leading to enhanced mechanical properties (Tserki, Zafeiropoulos, Simon, & Panayiotou, 2005).

3.1.1. Infrared spectroscopy

All composite membranes have been analyzed after complete drying. Fig. 1 evidences a significant reduction of the usual band at 3400 cm^{-1} as a result of esterification in POL and PHL, when compared to pristine lignins (not shown). In the case of PKL, only a weak signal is observed, caused by the remaining OH groups of the raw KL. The peak at 1730 cm^{-1} corresponds to the stretching vibration of the carbonyl (C=O) group present in the ester bond, due to the esterification of the hydroxyl groups. It appears in PKL, POL, and PHL.

A band is also present at 1760 cm^{-1} in the case of POL only. This has been reported as an evidence of propionyl groups in the form of propionic acid (Silverstein & Webster, 1998; Tserki et al., 2005). OL was not quenched with ether during esterification because it is totally soluble in it. Thus, although propionic anhydride is highly reactive, with a low probability that propionyl groups exist as anhydrides, there is a possibility in OL of a reversible reaction where some initial reagent could remain (Tserki et al., 2005).

In all cases, esterification reaction was also confirmed by the occurrence of a strong absorption at 1162–1229 cm^{-1}, attributed to the C–O stretching of the ester carboxyl groups (Silverstein & Webster, 1998).

3.1.2. UV spectroscopy

The amount q of free phenolic hydroxyls in lignins was quantified using the following relationship (Glasser & Jain, 1993; Gosselink et al., 2004; Lin & Dence, 1992; Nadji et al., 2009):

$$q = \frac{\Delta a_{max}}{\Delta \varepsilon} \times 1000 \quad (2)$$

where Δa_{max} ($L\,g^{-1}\,cm^{-1}$) is the difference of absorptivity between ionized and non-ionized compounds, and $\Delta\varepsilon$ ($L\,mol^{-1}\,cm^{-1}$) is the difference of molar absorptivity.

In a previous work (Manjarrez Nevárez et al., this issue), KL, HL and OL have been fully characterized, showing the presence of two different kinds of OH groups: p–p′ stilbene structure (Type IV) on one hand, and structures with saturated side chain (Type I) on the other hand. In the present case, absorption has been measured at its maximum, reached around 298 and 370 nm. Results obtained from the acquired spectra are listed in Table 2. The degree of substitution of propionic groups is related to the efficiency of the esterification process. Near total esterification has been achieved for HL and OL. For KL, there are more OH groups pertaining to type I. Such structures are less prone to esterification (Thielemans & Wool, 2005). Just like for the case of acetylation (Manjarrez Nevárez et al., this issue), KL is the least alkylated lignin of the series investigated here. This finding is consistent with IR results, showing the presence of a few OH groups in the case of PKL only.

Table 2
Phenol content of commercial and propionated lignins deduced from UV/Vis spectroscopy, and corresponding degree of substitution of propionic groups (DP).

Lignin	Type I OH ($mmol\,g^{-1}$)	Type IV OH ($mmol\,g^{-1}$)	% DP
KL	0.936	0.097	
PKL	0.142	0.045	81.77
OL	0.528	0.123	
POL	0.0	0.022	96.55
HL	0.424	0.156	
PHL	0.0	0.032	99.96

3.1.3. Gel permeation chromatography

Differences in solubility and thermoplastic character of lignins depend both on their chemical nature and on the way they have been separated. The raw lignins used in this study present considerable differences in terms of molecular weight and sulfur content (Manjarrez Nevárez et al., this issue). Thus, for instance, low molecular weight, sulfur-free, lignins (such as OL) show significantly higher solubility that those having higher molecular weight and sulfur content. In order to improve significantly the behavior of the other lignins, their chemical modification was required (Sjostrom & Alén, 1999). Moreover, our biosourced membranes were prepared in non-polar solvents, so it was necessary to enhance lignin solubility and hence its incorporation into the polymeric matrix during the evaporation–precipitation process.

GPC analyses were carried out for each modified lignin modified in order to look for any change of molecular weight. The weight (Mw) and number (Mn) average molecular weights, and polydispersity ($Mw\,Mn^{-1}$) of each propionated lignin are given in Table 3. As expected, an increase of Mw occurred due to the incorporation of the ester group, but Mn presented a different behavior. For PKL, Mn did not increase because KL presented a lower solubility in THF, making the GPC analysis uneasy in this solvent (Sjostrom & Alén, 1999). Thus, more lightweight KL molecules were dissolved than those having higher molecular weights, thus affecting the determination of Mn. As already observed (Manjarrez Nevárez et al., this issue), hydrolytic lignin is the one which presented the highest polydispersity index and the highest Mn and Mw after chemical modification. Higher esterifications lead to bigger particles, a key parameter for composite performance, as explained below.

Table 3
Number average molecular weight (Mn), weight average molecular weight (Mw), and polydispersity index (PDI) of propionated lignins.

Lignin	PDI	Mn	Mw
OL	2.02	571	1157
POL	2.38	1421	3389
KL	1.15	651	751
PKL	2.67	624	1671
HL	1.47	366	544
PHL	3.36	1853	6242

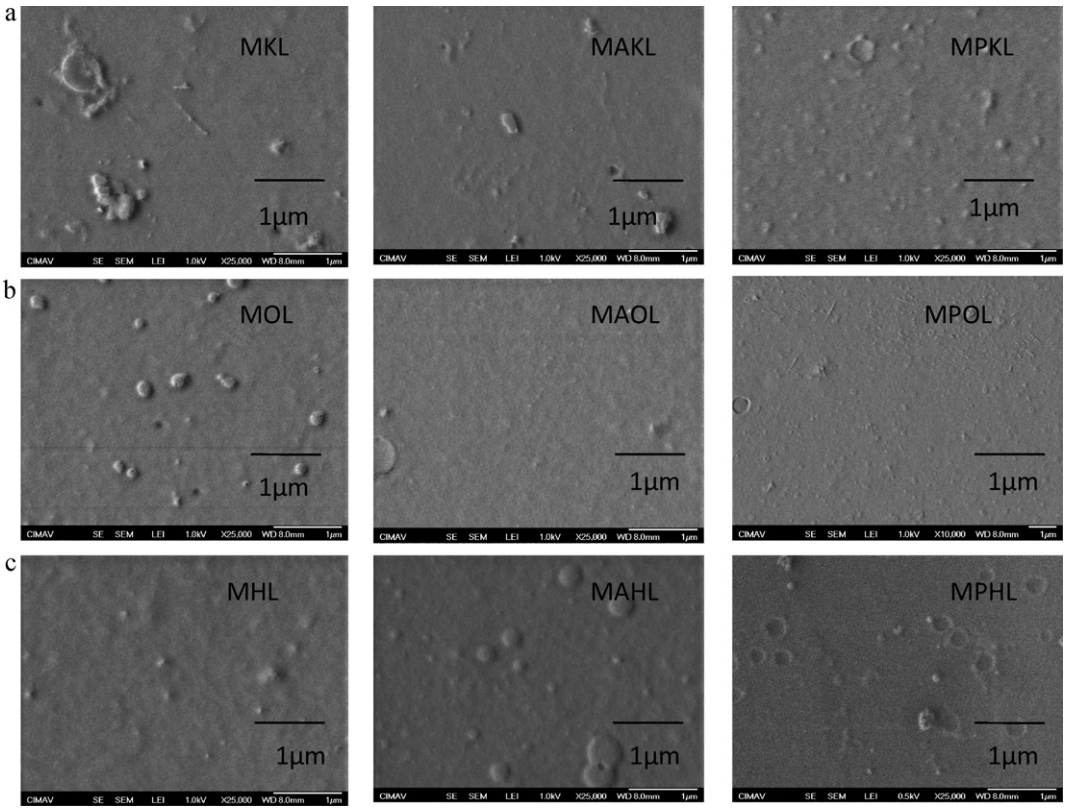

Fig. 2. FE-SEM micrographs of nanocomposites membranes (M), based on cellulose triacetate and 1 wt.% of propionated lignin (PKL, POL or PHL), and prepared at 35 °C and 70% relative humidity.

3.2. Nanocomposites characterization

3.2.1. Field emission scanning microscopy (FE-SEM)

Diffusion and transport in composites depend on the nature of the filler and on its degree of adhesion and compatibility with the polymeric matrix. A compromise needs to be found in the interaction among the polymer and the filler. When the filler is incompatible with the polymer, voids tend to occur at the interface, leading to an increase in the free volume of the system and consequently, in its permeability (George & Thomas, 2001). If the best mechanical properties are looked for, the best adhesion is desirable between matrix and filler, and voids should be avoided in the composite structure.

Some membranes were analyzed by classical SEM and many micrographies have been obtained. For all of them, a dense structure was evidenced, without clear difference from one material to another (Manjarrez Nevárez et al., this issue). Using FE-SEM, it was possible to analyze membrane-structure at the nanometer scale, demonstrating little differences between modified lignins. Fig. 2 shows FE-SEM micrographs of membranes obtained at 35 °C and 70% relative humidity, incorporating acetylated (Manjarrez Nevárez et al., this issue), propionated and raw Kraft, Organosolv and Hydrolytic lignins.

For all membranes obtained with KL and OL, see Fig. 2a and b, the homogeneity was clearly improved in the presence of chemically modified lignin. Increasing the chain length by esterification improved KL and OL dispersion in CTA. This behavior has been reported by Thielemans and Wool (2005) as well, who studied composites made from polystyrene and lignin. Modifying lignin with acetyl and propyl groups improved its incorporation into the matrix due to a correspondingly higher solubility. This finding was observed as far as the increase of molecular weight was limited. Thus, for membranes based on HL (Fig. 2c), a different behavior was noticed with ester group incorporation. HL decreased its solubility and related dispersion in CTA because its molecular weight increased much more, as shown from GPC analyses.

3.2.2. Mechanical properties

One of the main mechanisms of composite reinforcement is the segmental immobilization of the polymer chains of the matrix, caused by the interaction of the latter with the filler surface, where particle size is crucial for adhesion (Kalfus & Jancar, 2008). Nanoparticles incorporation into the polymeric matrix has been studied recently (Cai, Riedl, Zhang, & Wan, 2008; Jordan, Jacob, Tannenbaum, Sharaf, & Jasiuk, 2005; Tjong, 2006). It was observed that, at low filler loading, mechanical properties were greatly improved. Chen and Sun (2005) observed that agglomerated particles were poorly dispersed in the polymeric matrix. Composites' mechanical properties are indeed strongly related to good particle dispersion and strong interfacial adhesion (Eitan, Fisher, Andrews, Brinson, & Schadler, 2006; Wu et al., 2009).

Fig. 3 shows Young's modulus measured by traction of membranes obtained in various physicochemical conditions. Whatever the composition, the highest mechanical performances were obtained for nanocomposites prepared at 35 °C and 70% relative humidity. This result is in agreement with another work (Ballinas Casarrubias et al., 2006) dealing with CTA/activated carbon membranes. In all the cases, propionated Kraft lignin is the nanofiller leading to the highest Young's modulus, all other things being equal.

Strength and elongation at break were calculated for nanocomposites prepared at 35 °C and 70% RH, and based on either raw or propionated lignin. The corresponding curves and values are presented in Fig. 4 and in Table 4, respectively. Propionation significantly improved both modulus and tensile strength of membranes based on KL. Elongation at break decreased, as expected. KL was indeed the lignin presenting the worst incorporation into CTA,

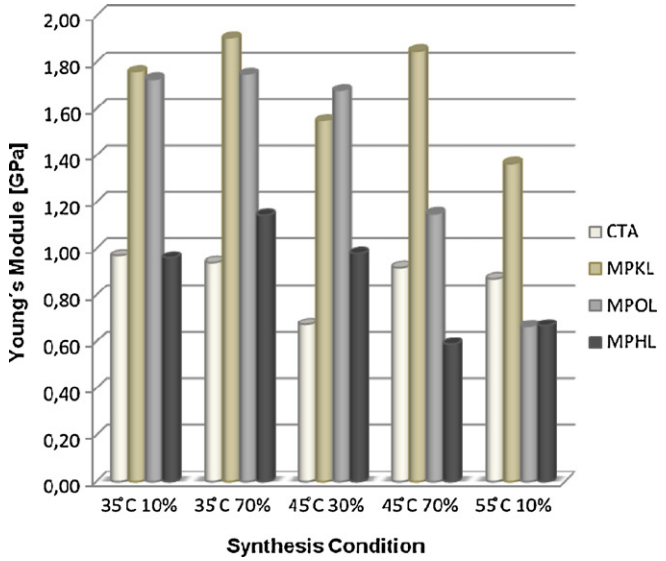

Fig. 3. Comparison of Young's modulus of membranes made in various temperature and RH conditions and based on either pure CTA or including propionated KL, OL or HL as nanofiller.

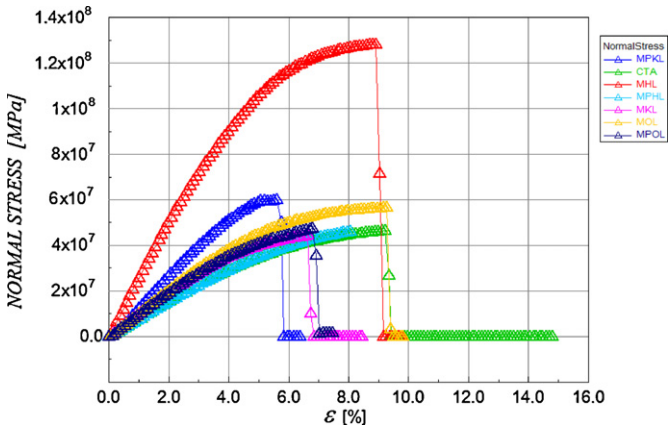

Fig. 4. Stress–strain curve for CTA, raw and propionated lignin nanocomposites.

mainly because of its high hydroxyl content. When propionated, adhesion and surface affinity increased significantly, propyl groups interacting with acetate group in cellulose through London dispersion forces.

In contrast, propionation decreased all the mechanical characteristics of membranes prepared from the two other kinds of lignin: OL and HL. The effect is rather low with OL, but significant in the case of HL, for which the initial high molecular weight may account for

Table 4
Young's modulus, elongation at break and tensile strength for CTA and nanocomposites membranes based on raw (MKL, MOL and MHL) and propionated lignin (MPKL, MPOL and MPHL), prepared at 35 °C and 70% RH.

Sample	Young's modulus (GPa)	Elongation at break (%)	Tensile strength (MPa)
MKL	0.9	6.64	41.19
MPKL	1.9	5.61	60.3
MOL	1.2	9.26	56.7
MPOL	1.15	6.79	47.3
MHL	2.98	8.91	128
MPHL	1.14	7.90	45.8
CTA	0.94	9.20	46.4

Table 5
Transmembrane flux, contact angle, moisture content and root mean square roughness for CTA and propionated lignin nanocomposites.

Sample	Flux ($L\,m^{-2}\,h^{-1}\,bar^{-1}$)	Contact angle (°)	Humidity (%)	R_{rms} (nm)
MKL	5.89	47.7	2.46	26.6
MPKL	2.77	61.4	1.50	5.49
MOL	1.50	59.3	1.84	3.55
MPOL	0.17	63.2	1.25	2.43
MHL	0.19	59.1	1.56	5.53
MPHL	0.03	75.4	1.30	16.05
CTA	0.22	52.6	1.95	1.99

the exceptionally high modulus and tensile strength. This finding is explained by the corresponding increase of particle size, which is substantial in the case of PHL, which decreased the quality of the adhesion between filler and matrix. The results of Table 4 thus clearly show that good membranes are based on a compromise between antagonistic effects, and also show how difficult it is to foresee which effect will control the properties of the resultant nanocomposites.

3.2.3. Atomic force microscopy (AFM)

AFM was used to measure the surface roughness of membranes, and images of some of the nanocomposite membranes are shown in Fig. 5. Color intensity shows the vertical profile of the sample. The light region is the highest point and the dark region corresponds to a depression in the material. Roughness is one of the most important surface properties because of its influence on flow properties and local mass transfer (Gordano, Arcella, & Drioli, 2004). It also affects contact angle and membrane hydrophilicity (Rosa & Pinho, 1997).

Incorporation of lignin nanoparticles into CTA accounts for the changes in surface roughness. This propriety could be measured using the WSxM software supplied with the AFM. The corresponding data: roughness data (R_{rms}) and other parameters obtained, are given in Table 5. For KL, an obvious smoothing of the surface was observed after esterification. R_{rms} decreased as side chain length increased. For OL, the same trend was observed. However, in the case of HL, and as mentioned before, its increase in molecular weight affected particle incorporation into the polymer matrix (Chen & Sun, 2005).

3.2.4. Contact angle and TGA

Contact angle measurements give information about the affinity of a liquid with a solid surface. If water is used to measure the contact angle, θ, the hydrophobic ($\theta > 90°$) or hydrophilic ($\theta < 90°$) character of the surface can be inferred. CTA is a highly hydrophilic polymer comprising adsorbed water in its structure (Fan, Wang, Sun, Wang, & Wang, 2008). The amount of water that can be retained by each sample has been measured by thermogravimetric analysis. Data of contact angle and humidity are listed in Table 5.

Chemical modification modified roughness and wettability of the resultant membrane. Kraft lignin was the most hydrophilic one. After propionation, nanocomposite hydrophobicity increased, as evidenced by the higher contact angle and lower resultant moisture content. Thus, MPKL presented a hydrophobic character compared to CTA films. When KL and acetylated KL were used as nanofiller in CTA-based membranes, an average of 2% of humidity was reported (Manjarrez Nevárez et al., this issue). Table 5 shows that the results of propionation are slightly better from that point of view. Propionation also modified roughness. As lignin was modified, nanoparticle incorporation was easier, producing a more homogeneous material.

For OL, hydrophobicity and roughness of the membranes were slightly modified by chemical modification, but the trends are the

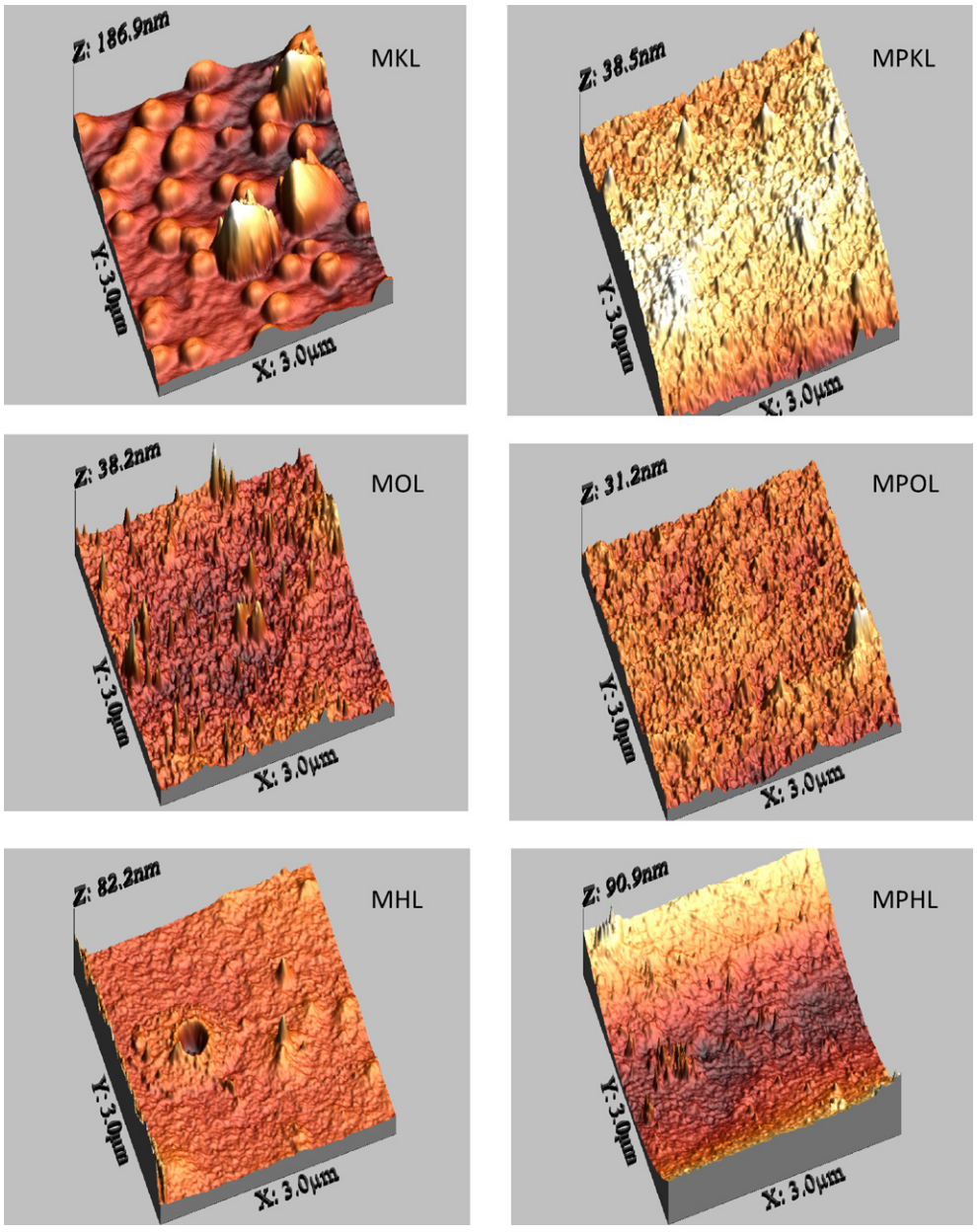

Fig. 5. Topographic images obtained by AFM for raw and propionated lignin nanocomposites.

same as those observed for KL. Fluxes are of the same order for propionated, acetylated and raw MOL (Manjarrez Nevárez et al., this issue). In the case of HL, propionation led to the highest hydrophobicity and to correspondingly very low moisture content, as expected. However, the poorer adhesion of PHL nanoparticles with CTA matrix led to a heterogeneities and hence to high roughness of the films.

3.2.5. Permeability properties

Membrane technology is traditionally used for groundwater treatment. Common processes are, depending on the driving force, divided into microfiltration (MF), ultrafiltration (UF), nanofiltration (NF) and reverse osmosis (RO). MF and UF separation looks like mechanical sieving, while NF and RO use capillary flow or solution diffusion (Brandhube & Amy, 2001). In nanofiltration, anion separation is based not only on different diffusion rates throughout the membrane, but also on repulsion (Donnan exclusion) between anions in solution and the surface groups, which is higher for multivalent anions (Levenstein, Hasson, & Semiat, 1996). This mechanism presents an advantage over RO, because allowing high ion rejections as RO but with higher flows (Uddin, Mozumder, Figoli, Drioli, & Islam, 2007).

Table 5 shows that the flux measured throughout membranes prepared from propionated lignins decreased dramatically, by two orders of magnitude, from MPKL to MPOL and MPHL. The flux is known to be related to both roughness and hydrophilicity (Ghosh, Jain, & Glasser, 2000; Hirose, Ito, & Kamiyama, 1996) but, given the spreading of the R_{rms} values presented in Table 5, the flux drop seems to be the most sensitive to the increase of contact angle. Because of so different transport properties, only the membranes presenting fluxes higher than 1 L m^{-2} h^{-1} bar^{-1} were tested in NF, whereas the others were investigated in RO, see below.

There are many works dealing with fluoride and arsenic removal from synthetic solutions using RO and NF processes (Figoli et al., 2010; Harisha, Hosamani, Keri, Nataraj, & Aminabhavi, 2010; Kartinen & Mar-

tin, 1995; Pérez Sicairos, Wai Lin, Félix Navarro, & Espinoza Gómez, 2009), revealing high removal percentages. Nevertheless, only a few works dealing with natural groundwater have been reported (Brandhube & Amy, 2001; Meenakshi, Garg, Kavita, Renuka, & Malik, 2004; Schneiter & Middlebrooks, 1983; Wang, Liu, Li, & Ma, 2009; Waypa, Elimelech, & Hering, 1997), for which membrane effectiveness may be affected by suspended solids (Meenakshi et al., 2004). Table 6 shows rejection results, as defined by Eq. (1), for arsenic, fluoride, sodium, calcium and magnesium. In all cases, rejection of cations is higher than that of anions. Nanocomposites with raw lignins (MKL and MOL) improved their permeability properties with propionation (MPKL and MPOL), except for arsenic which was slightly less rejected.

It has been reported that divalent anions and cations in groundwater present antagonistic effects on arsenic removal. Brandhube and Amy (2001) indeed observed that Ca and Mg reduce arsenate rejection to almost zero. On the other hand, organic matter found in groundwater may significantly complex both Ca and Mg. The high affinity of Ca^{2+} for binding sites of humic acid has been observed (Mathuthu & Ephraim, 1993; Thurman, 1985). When divalent ions are complexed by organic matter, their distribution at the membrane surface might be altered, producing the opposite effect on arsenic removal, i.e. an easier rejection. Additionally, As in water can form organic and inorganic species (Del Razo, Arellano, & Cebrián, 1990). There are also differences in molecular size and charge which are important in membrane process separation. Arsenic species include pentavalent arsenic as $H_2AsO_4^-$ ($pK_{a_1} = 2.22$), $HAsO_4^{2-}$ ($pK_{a_2} = 6.94$) and $HAsO_4^{3-}$ ($pK_{a_3} = 9.13$). At typical pH values of drinking water (between 6 and 9), trivalent arsenic is found as neutral species: H_3AsO_3 (Akbari, Rashidi Mehrabadi, & Torabian, 2010). Hence, electrically charged membrane surfaces may reject or incorporate ionic compounds, depending on the charges of the latter, by a solution-diffusion mechanism. Lignin may influence the distribution of charges all over the membrane surface, and induce different behaviors compared to CTA alone.

Further studies have to be performed to find out the specificities of each material, even though surface potential could be estimated by SKPM technique.

3.2.6. Scanning Kelvin probe microscopy (SKPM)

SKPM has become a very strong tool in material science (Kitamura, Suzuki, & Iwatsuki, 1998; Muller et al., 2004; Sykes & Doherty, 2008), giving up a surface mapping of electrostatic potential (Koley, Spencer, & Bhangale, 2001; Nichols, Gundlach, & Jackson, 2003). Electrical properties have an important role in the rejection of charged species in membrane applications such as water softening and heavy metal removal (Elimelech, Zhu, Childress, & Hong, 1997). Increasing membrane charge may improve ion rejection for nanofiltration (NF) and reverse osmosis (RO) processes. If membrane is electrically charged, electrostatic interaction becomes significant for ion removal (Elimelech et al., 1997).

Nanocomposites which presented the best flows were characterized by SKPM for getting information about their electrical potential, namely MKL, MPKL, MAKL, MOL and CTA membranes obtained at 35 °C and 70% humidity. The resultant pictures are shown in Fig. 6(a–e), comparing topographic images and potential mappings. In all cases, clear correlations may be observed between the two kinds of pictures. Dark zones of SPKM images correspond to a difference of potential between surface and AFM tip, whereas no difference corresponds to bright zones. For all nanocomposites analyzed, electrical charges were evidenced all over the surfaces.

Nanofiltration membranes presented a surface electrical potential which could be attributed to lignin incorporation into the polymeric matrix. For instance, in CTA membranes, no indication

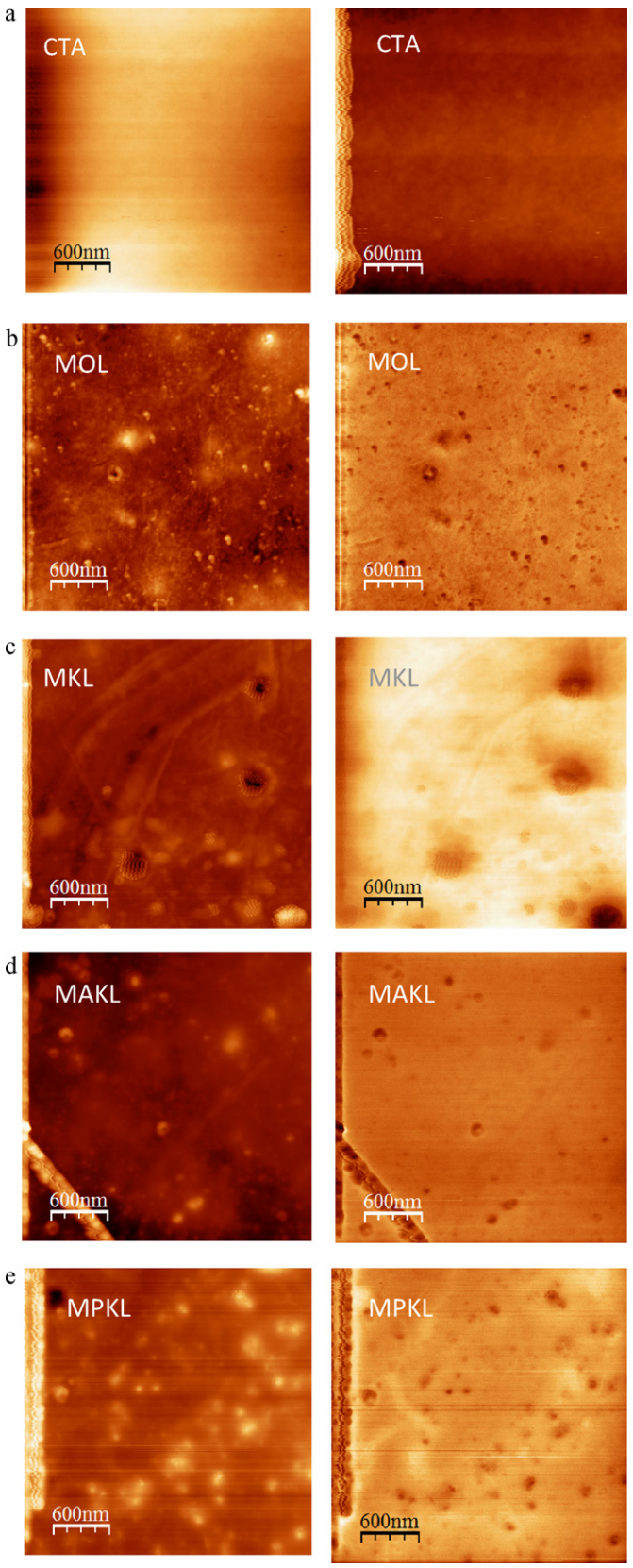

Fig. 6. SKPM views of CTA and nanofiltration composites (MOL, MKL, MAKL and MPKL). Topography and surface potential mapping are shown at the left and at the right side of the figure, respectively.

Table 6
Pressure at which the steady state flow is reached, process of membrane synthesis, and arsenic, fluoride, calcium and magnesium percentage of rejection for CTA and nanocomposites based on raw and propionated lignins.

Sample	Pressure (bar)	Membrane process	Rejection As (%)	Rejection F (%)	Rejection Ca (%)	Rejection Mg (%)	Rejection Na (%)
MKL	11.79	NF	17.80	14.29	36.11	31.82	12.0
MPKL	16.55	NF	15.06	30.91	46.76	54.55	23.6
MOL	22.07	NF	17.13	5.74	33.33	27.27	26.60
MPOL	20.69	RO	22.80	32.86	41.67	40.91	35.0
MHL	26.21	RO	26.32	30.71	51.85	45.45	40.0
MPHL	27.59	RO	19.77	35.71	52.78	43.18	42.4
CTA	21.72	RO	25.40	27.14	37.96	31.82	44.6

of electrical potential at the surface of the material was found (see Fig. 6c).

4. Conclusions

Propionation allowed incorporating lignin nanoparticles to CTA polymer matrix. Hydrolytic lignin showed the best mechanical performance, revealing that particle size is crucial for getting the best filler-polymer adhesion. Nevertheless, for propionated lignin, roughness was the lowest for MPKL and MPOL, as shown by AFM studies. All lignin nanocomposites were electrically charged, by contrast with pure CTA.

Membrane performances were tested in nanofiltration or reverse osmosis, depending on the kind of CTA–lignin composite. Higher propionation of lignin induced lower wettability and lower fluxes of nanocomposites. KL is the less esterified lignin of the three types tested. MPKL composite present the highest flux than MPOL and MPHL. Nevertheless, MPKL Young's module is higher than MKL, demonstrating the effectiveness of esterification treatment of lignins. In groundwater treatment, total anion and cation concentration affected membrane performance, inducing lower rejection values.

Acknowledgements

The French authors from IJL laboratory gratefully acknowledge the financial support of the CPER 2007-2013 "Structuration du Pôle de Compétitivité Fibres Grand'Est" (Competitiveness Fibre Cluster), through local (Conseil Général des Vosges), regional (Région Lorraine), national (DRRT and FNADT) and European (FEDER) funds. L. Manjarrez thanks CONACYT for her Ph.D. grant. G. Gonzalez to CONACYT for funding (SEP CONACYT-CB-2005-C01-46431). The authors are grateful with the Laboratorio Nacional de Nanotecnología for AFM, SKPM, SEM and FE-SEM characterization. We would also thank W. Antunez, M. Mendoza and K. Campos for all their technical support in sample characterization.

References

Akbari, H. R., Rashidi Mehrabadi, A., & Torabian, A. (2010). Study on nonofiltration efficiency in arsenic removal from drinking water. *Iran Journal of Environmental Health Science and Engineering*, *7*, 273–278.

Alemdar, A., & Sain, M. (2008). Biocomposites from wheat straw nanofibers: Morphology, thermal and mechanical properties. *Composite Science and Technology*, *68*, 557–565.

Alexy, P, Kosikova, B., & Podstranska, G. (2000). The effect of blending lignin with polyethylene and polypropylene on physical properties. *Polymer*, *41*, 4901–4908.

Andrade Molinar, C. (2007). Biofouling characterization of membranes for waste water treatment, Unpublished Manuscript, Universidad Autónoma de Chihuahua, Chihuahua, Chih. México.

Arthanareeswaran, G., Thanikaivelan, P., Srinivasn, K., Mohan, D., & Rajendran, M. (2004). Synthesis, characterization and thermal studies on cellulose acetate membranes with additive. *European Polymer Journal*, *40*, 2153–2159.

Asatekin, A., Kang, S., Elimelech, M., & Mayes, A. M. (2007). Anti-fouling ultrafiltration membranes containing polyacrylonitrile graft poly(ethylene oxide) comb copolymer additives. *Journal of Membrane Science*, *298*, 136–146.

Baker, R. W. (2004). Reverse osmosis. In *Membrane technology and application*. England: John Wiley & Sons., pp. 197–198.

Ballinas Casarrubias, L., Terrazas Bandala, L. P., Ibarra Gómez, R., Mendoza Daurte, M. E., Manjarrez Nevárez, L. A., & González Sánchez, G. (2006). Structural and performance variation of activated carbon polymer films. *Polymers for Advanced Technology*, *17*, 991–999.

Baumberger, S., Lapierre, C., Monties, B., & Della Valle, G. (1998). Use of kraft lignin as filler for starch film. *Polymer Degradation and Stability*, *59*, 211–213.

Brandhube, P., & Amy, G. (2001). Arsenic removal by a charged ultrafiltration membrane influences of membrane operating conditions and water quality on arsenic rejection. *Desalination*, *140*, 1–14.

Cai, X., Riedl, B., Zhang, S. Y., & Wan, H. (2008). The impact of the nature of nanofillers on the performance of wood polymer nanocomposites. *Composites: Part A*, *39*, 727–737.

Canetti, M., & Bertini, F. (2007). Supermolecular structure and thermal properties of poly(ethylene terephthalate)/lignin composites. *Composite Science and Technology*, *67*, 3151–3157.

Chen, Y., Liu, C., Chang, P. R., Cao, X., & Anderson, D. P. (2009). Bionanocomposites based on pea starch and cellulose nanowhiskers hydrolyzed from pea hull fibre: Effect of hydrolysis time. *Carbohydrate Polymer*, *76*, 607–615.

Chen, B., & Sun, K. (2005). Poly (ε-caprolactone)/hydroxyapatite composites: Effects of particle size, molecular weight distribution and irradiation on interfacial interaction and properties. *Polymer Testing*, *24*, 64–70.

Connors, W. J., Sarkanen, S., & McCarthy, J. L. (1980). Gel chromatography and association complexes of lignin. *Holzforschung*, *34*, 80–85.

Del Razo, L. M., Arellano, M. A., & Cebrián, M. E. (1990). The oxidation states of arsenic in well-water from a chronic arsenicism area of Northern Mexico. *Environmental Pollution*, *64*, 143–153.

Drioli, E., & Romano, M. (2001). Progress and new perspectives on integrated membrane operations for sustainable industrial growth. *Industrial and Engineering Chemistry Research*, *40*, 1277–1300.

Edgar, K. J, Buchanan, C. M., Debenham, J. S., Rundquist, P. A., Seiler, B. D., Shelton, M. C., et al. (2001). Advance in cellulose ester performance and application. *Progress in Polymer Science*, *26*, 1605–1688.

Eitan, A., Fisher, F. T., Andrews, R., Brinson, L. C., & Schadler, L. S. (2006). Reinforcement mechanisms in MWCNT-filled polycarbonate. *Composite Science and Technology*, *66*, 1159–1170.

Elimelech, M., Zhu, X., Childress, A. E., & Hong, S. (1997). Role of membrane surface morphology in colloidal fouling of cellulose acetate and composite aromatic polyamide reverse osmosis membranes. *Journal of Membrane Science*, *127*, 101–109.

El-Saied, H., Basta, A. H., Barsoulm, B. N., & Elberry, M. M. (2003). Cellulose membranes for reverse osmosis Part I. RO cellulose acetate membranes including a composite with polypropylene. *Desalination*, *159*, 171–181.

Fan, Z., Wang, Z., Sun, N., Wang, J., & Wang, S. (2008). Performance improvement of polysulfone ultrafiltration membrane by blending with polyaniline nanofibers. *Journal of Membrane Science*, *320*, 363–371.

Faust, S. D., & Aly, O. M. (1998). *Chemistry of water treatment* (2nd ed.). New York: CRC Press.

Fierro, V., Torné Fernández, V., & Celzard, A. (2006). Kraft lignin as a precursor for microporous activated carbons prepared by impregnation with orthophosphoric acid: Synthesis and textural characterisation. *Microporous and Mesoporous Materials*, *92*, 243–250.

Figoli, A., Cassano, A., Criscuoli, A., Mozumder, M. S. I., Uddin, M. T., Islam, M. A., et al. (2010). Influence of operating parameters on the arsenic removal by nanofiltration. *Water Research*, *44*, 97–104.

George, S. C., & Thomas, S. (2001). Transport phenomena through polymeric system. *Progress in Polymer Science*, *26*, 985–1017.

Ghosh, I., Jain, R. K., & Glasser, W. G. (2000). Blends of biodegradable thermoplastics with lignin esters. In W. G. Glasser, R. A. Northey, & T. P. Schultz (Eds.), *Lignin: Historical, biological, and materials perspectives* (pp. 331–350). Washington, DC: ACS Symposium Series.

Glasser, W. G., & Jain, R. K. (1993). Lignin derivatives: I. Alkanoates. *Holzforschung*, *47*, 225–233.

Goldschmid, O. (1954). Determination of phenolic hydroxyl content of lignin preparations by ultraviolet spectrophotometry. *Analytical Chemistry*, *26*, 1421–1423.

Gordano, A., Arcella, V., & Drioli, E. (2004). New HYFLON AD composite membranes and AFM characterization. *Desalination*, *163*, 127–136.
Gosselink, R. J. A., Abächerli, A., Semke, H., Malherbe, R., Käuper, P., Nadif, A., et al. (2004). Analytical protocols for characterisation of sulphur-free lignin. *Industrial Crops and Products*, *19*, 271–281.
Gregorová, A., Cibulková, Z., Kosiková, B., & Símon, P. (2005). Stabilization effect of lignin in polypropylene and recycled polypropylene. *Polymer Degradation and Stability*, *89*, 553–558.
Haddad, R., Ferjani, E., Roudesli, M. S., & Deratani, A. (2004). Properties of cellulose acetate nanofiltration membranes. Application to brackish water desalination. *Desalination*, *167*, 403–409.
Harisha, R. S., Hosamani, K. M., Keri, R. S., Nataraj, S. K., & Aminabhavi, T. M. (2010). Arsenic removal from drinking water using thin film composite nanofiltration membrane. *Desalination*, *252*, 75–80.
Hirose, M., Ito, H., & Kamiyama, Y. (1996). Effect of skin layer surface structures on the flux behaviour of RO membranes. *Journal of Membrane Science*, *121*, 209–215.
Horcas, I., Fernandez, R., Gomez Rodriguez, J. M., Colchero, J., Gomez Herrero, J., & Baro, A. M. (2007). WSxM: A software for scanning probe microscopy a tool for nanotechnology. *Review of Scientific Instrument*, *78*, 013705.
Jordan, J., Jacob, K. I., Tannenbaum, R., Sharaf, M. A., & Jasiuk, I. (2005). Experimental trends in polymers nanocomposites- a review. *Materials Science and Engineering A*, *393*, 1–11.
Kalfus, J., & Jancar, J. (2008). Reinforcing mechanisms in amorphous polymer nanocomposites. *Composite Science and Technology*, *68*, 3444–3447.
Kamel, S. (2007). Nanotechnology and its applications in lignocellulosic composites, a mini review. *Express Polymer Letter*, *1*, 546–575.
Kartinen, E. O., & Martin, C. J. (1995). An overview of arsenic removal processes. *Desalination*, *10*, 379–388.
Kitamura, S., Suzuki, K., & Iwatsuki, M. (1998). Observation of silicon surfaces using ultrahigh vacuum noncontact atomic force microscope. *Japanese Journal of Applied Physics*, *373*, 765–3768.
Kiziltas, A., Gardner, D. J., Han, Y., & Yang, H. S. (2010). Thermal properties of microcrystalline cellulose-filled PET–PTT blend polymer composites. *Journal of Thermal Analysis and Calorimetry*, *103*, 163–170.
Koley, G., Spencer, M. G., & Bhangale, H. R. (2001). Cantilever effects on the measurement of electrostatic potentials by scanning Kelvin probe microscopy. *Applied Physics Letters*, *79*, 545–548.
Kosutic, K., Kstelan Kunst, L., & Kunst, B. (2000). Porosity of some commercial reverse osmosis and nanofiltration polyamide thin film composite membrane. *Journal of Membrane Science*, *168*, 101–108.
Le Digabel, F., & Avéous, L. (2006). Effects of lignin content on the properties of lignocelluloses-base biocomposites. *Carbohydrate. Polymer*, *66*, 537–545.
Levenstein, R., Hasson, D., & Semiat, R. (1996). Utilization of the Donnan effect for improving electrolyte separation with nanofiltration membranes. *Journal of Membrane Science*, *116*, 77–92.
Lin, S. Y., & Dence, C. W. (1992). Ultraviolet spectrophotometry. In *Methods in lignin chemistry*. Heidelberg, Germany: Springer-Verlag., pp. 217–231.
Manjarrez Nevárez, L., Ballinas Casarrubias, L., Celzad, A., Fierro, V., Torres Muñoz, V., Camacho Dávila, A., et al. Biopolymer-based nanocomposites: Effect of lignin acetylation in cellulose triacetate membrane, this issue.
Mathuthu, A., & Ephraim, J. (1993). Calcium binding by fulvic acid studied by an ion selective electrode and an ultrafiltration method. *Talanta*, *40*, 521–526.
Meenakshi, Garg, V. K., Kavita, Renuka, & Malik, A. (2004). Groundwater quality in some villages of Haryana, India: Focus on fluoride and fluorosis. *Journal of Hazardous Material*, *106*, 85–97.
Mercade, M. E., & Manresa, M. A. (1994). The use of agroindustrial by-products for biosurfactant production. *Journal of the American Oil Chemist's Society*, *71*, 61–64.
Muller, K., Goryachko, A., Burkov, Y., Schwiertz, C., Ratzke, M., Koblec, J., et al. (2004). Scanning Kelvin probe and photoemission electron microscopy of organic source-drain structures. *Synthetic Metals*, *146*, 377–382.
Nadji, H., Diouf, P. N., Benaboura, A., Bedard, Y., Riedl, B., & Stevanovic, T. (2009). Comparative study of lignins isolated from Alfa grass (*Stipa tenacissima* L.). *Bioresource Technology*, *100*, 3585–3592.
Nichols, J. A., Gundlach, D. J., & Jackson, T. N. (2003). Potential imaging of pentacene organic thin-film transistors. *Applied Physics Letters*, *83*, 2366–2368.
Oksman, K., Mathew, A. P., Bondeson, D., & Kvien, I. (2006). Manufacturing process of cellulose whiskers/polylactic acid nanocomposites. *Composite Science and Technology*, *66*, 2776–2784.
Pandey, A., Soccol, C. R., Nigam, P., & Soccol, V. T. (2000). Biotechnological potential of agro-industrial residues. I: Sugarcane bagasse. *Bioresource Technology*, *74*, 69–80.
Park, H. M., Misra, M., Drzal, L. T., & Mohanty, A. K. (2004). "Green" nanocomposites from cellulose acetate bioplastic and clay: Effect of eco-friendly triethyl citrate plasticizer. *Biomacromolecules*, *5*, 2281–2288.
Pérez Sicairos, S., Wai Lin, S., Félix Navarro, R. M., & Espinoza Gómez, H. (2009). Rejection of As(III) and As(V) from arsenic contaminated water via electro-cross-flow negatively charged nanofiltration membrane system. *Desalination*, *249*, 458–465.
Pouteau, C., Dole, P., Cathala, B., Averous, L., & Boquillon, N. (2003). Antioxidant properties of lignin in polypropylene. *Polymer Degradation and Stability*, *81*, 9–18.
Pucciariello, R., Villani, V., Bonini, C., D'Auria, M., & Vetere, T. (2004). Physical properties of Straw lignin based polymer blends. *Polymer*, *45*, 4159–4169.
Rosa, M. J., & Pinho, M. N. (1997). Membrane surface characterisation by contact angle measurements using the immersed method. *Journal of Membrane Science*, *131*, 167–180.
Ruehr, T., Ruehr, E., Gong, T. R., & Theodore, M. G. (2010). Pre-treatment reverse osmosis water recovery method for brine retentate metal removal. Unpublished manuscript. US Patent.
Schneiter, R. W., & Middlebrooks, E. J. (1983). Arsenic and fluoride removal from groundwater by reverse osmosis. *Environment International*, *9*, 289–291.
Secretaria del Medio Ambiente y Recursos Naturales. (2001a). Water analysis determination of fluorine in natural, wastewater and wastewater treated test method, Norma Mexicana. NMX-AA-077-SCFI-2001.
Secretaria del Medio Ambiente y Recursos Naturales. (2001b). Water analysis determination of metals by atomic absorption natural, drinking, wastewater and wastewater treated test method, Norma Mexicana. NMX-AA-051-SCFI-2001.
Serry, F. M., Kjoller, K., Thornton, J. T., Tench, R. J., & Cook, D. (2004). Electric force microscopy, surface potential imaging and surface electrical modification with the atomic force microscope (AFM), *Vecco Instrument Inc*. AN27.
Silverstein, R. M., & Webster, F. X. (1998). *Spectrometric identification of organic compounds* (6th ed.). New York: Wiley.
Sims, R., Michael, T., Jack, S., & Warren, M. (2008). From 1st- to 2nd-generation biofuel technologies: An overview of current industry and RD&D activities. *International Energy Agency and Organization for Economic Cooperation and Development*, 35–37.
Sjostrom, E., & Alén, R. (1999). *Analytical methods in wood chemistry, pulping and papermaking*. Heidelberg, Germany: Springer Verlag.
Stewart, D. (2008). Lignin as a base material for materials applications: Chemistry, application and economics. *Industrial Crops and Products*, *27*, 202–207.
Sykes, J. M., & Doherty, M. (2008). Interpretation of Scanning Kelvin Probe potential maps for coated steel using semi-quantitative current density maps. *Corrosion Science*, *50*, 2773–2778.
Thielemans, W., & Wool, R. P. (2005). Lignin esters for use in unsaturated thermosets: Lignin modification and solubility. *Biomacromolecules*, *6*, 1895–1905.
Thurman, E. M. (1985). Organic process, reactions, and pathways in natural waters. In *Organic geochemistry of natural waters*. Netherlands: Kluwer Academic Publishers., p. 415.
Tjong, S. C. (2006). Structural and mechanical properties of polymer nanocomposites. *Materials Science and Engineering: R: Reports*, *53*, 73–197.
Tserki, V., Zafeiropoulos, N. E., Simon, F., & Panayiotou, C. (2005). A study of the effect of acetylation and propionylation surface treatments on natural fibres. *Composites: Part A*, *36*, 1110–1118.
Uddin, M. T., Mozumder, S. I., Figoli, A., Drioli, E., & Islam, M. A. (2007). Arsenic removal by conventional and membrane technology: An overview. *Indian Journal of Chemical Technology*, *14*, 441–450.
Wang, L., Li, J., Li, Y., & Chen, C. (2007). Separation of dimethyl carbonate/methanol mixtures by pervaporation with poly(acrylic acid)/poly(vinyl alcohol) blend membranes. *Journal of Membrane Science*, *305*, 238–246.
Wang, X., Liu, W., Li, D., & Ma, W. (2009). Arsenic (V) removal from groundwater by GE-HL nanofiltration membrane: Effects of arsenic concentration, pH, and co-existing ions. *Frontiers of Environmental Science and Engineering China*, *3*, 428–433.
Waypa, J. J., Elimelech, M., & Hering, G. J. (1997). Arsenic removal by RO and NF. *Journal-American Water Work Association*, *89*, 102–114.
Wu, R. L., Wang, X. L., Li, F., Li, H. Z., & Wang, Y. Z. (2009). Green composite films prepared from cellulose, starch and lignin in room temperature ionic liquid. *Bioresource Technology*, *100*, 2569–2574.